DATA PAPER

Measuring stellar populations, dust attenuation and ionized gas at kpc scales in 10010 nearby galaxies using the integral field spectroscopy from MaNGA

Niu Li(李牛)[†] and Cheng Li(李成)[‡]

Department of Astronomy, Tsinghua University, Beijing 100084, *China*

(Received 19 November 2022; revised manuscript received 3 January 2023; accepted manuscript online 6 January 2023)

As one of the three major experiments of the fourth-generation Sloan Digital Sky Survey (SDSS-IV), the Mapping Nearby Galaxies at Apatch Point Observatory (MaNGA) survey has obtained high-quality integral field spectroscopy (IFS) with a resolution of 1–2 kpc for $\sim 10^4$ galaxies in the local universe during its six-year operation from July 2014 through August 2020. It is crucial to reliably measure the physical properties of the different components in each spectrum before one can use the data for any scientific study. In the past years we have made lots of efforts to develop a novel technique of full spectral fitting, which estimates a model-independent dust attenuation curve from each spectrum, thus allowing us to break the degeneracy between dust attenuation and stellar population properties when fitting the spectrum with stellar population synthesis models. We have applied our technique to the final data release of MaNGA, and obtained measurements of stellar population properties and emission line parameters, as well as the kinematics and dust attenuation of both stellar and ionized gas components. In this paper we describe our technique and the content and format of our data products. The whole dataset is publicly available in Science Data Bank with the link https://doi.org/10.57760/sciencedb.j00113.00088.

Keywords: integral field spectroscopy, stellar populations, dust attenuation, ionized gas

PACS: 98.10.+z, 98.35.Ln, 98.38.Hv, 98.38.Cp **DOI:** 10.1088/1674-1056/acb0ba

1. Introduction

In the last two decades, astronomers have conducted a number of surveys that provide integral field spectroscopy (IFS) for studying galaxies at kpc or even sub-kpc scales, such as SAURON,[1] DiskMass,[2] ATLAS^{3D},[3] the Sydney-AAO Multi-object Integral field spectrograph (SAMI),[4] the Calar Alto Legacy Integral Field Area (CALIFA),[5] Mapping Nearby Galaxies at Apatch Point Observatory (MaNGA),[6] Gas-Stripping Phenomena in galaxies (GASP)[7] and Physics at High Angular resolution in Nearby Galaxies with the Multi-Unit Spectroscopic Explorer (PHANGS-MUSE).[8] Though with small sample sizes (∼100–200 galaxies), early IFS surveys (e.g., SAURON, ATLAS^{3D}, DiskMass) demonstrated the great power of IFS data to study internal properties of galaxies and motivated the many follow-up larger surveys. The CALIFA survey observed a sample of ∼600 nearby galaxies, making a significant step forward in spatially resolved spectroscopic studies of galaxies, while the SAMI survey took a further step forward with a significant improvement in sample size (∼3000 galaxies).

As the largest IFS survey to date, the MaNGA survey made a big step forward again by obtaining high-quality IFS data for more than 10 thousands galaxies across a wide range in stellar mass, color, star formation rate (SFR) and environment, and with a long and continuous wavelength coverage from ∼3600 Å up to 10300 Å. Raw datacubes are processed by the MaNGA Data Reduction Pipeline (DRP)[9] that have an effective spatial resolution of 2.5″, corresponding to 1–2 kpc at the median redshift $\langle z \rangle = 0.03$. The DRP products of all the MaNGA galaxies are released as part of the SDSS Data Release 17 (SDSS-DR17).[10] A "project-led" MaNGA Data Analysis Pipeline (DAP)[11] has been developed and applied to the DRP data to measure stellar kinematics, fluxes and kinematics of emission lines and continuum spectral indices. In addition, a number of full spectral fitting codes are applied to the MaNGA spectra in order to estimate stellar population properties (e.g., stellar age, stellar metallicity and star formation histories), such as `pPXF` developed by Cappellari & Emsellem (2004),[12] `STARLIGHT` by Cid-Fernandes *et al.* (2005),[13] `Pipe3D` by Sánchez *et al.* (2016),[14] `Firefly` by Wilkinson *et al.* (2017).[15,16] Some of these products are also included in SDSS-DR17 as "value-added catalogs" (VACs), contributed by members of the MaNGA team.

A well-known difficulty in measuring stellar population properties from full spectral fitting is the strong degeneracy between dust attenuation and stellar population properties. In most cases, a parameterized model is adopted to represent the dust attenuation law and is included as one of the many free

[†]Corresponding author. E-mail: liniu@mail.tsinghua.edu.cn
[‡]Corresponding author. E-mail: cli2015@tsinghua.edu.cn

© 2023 Chinese Physical Society and IOP Publishing Ltd

parameters during the spectral fitting process. To overcome this difficulty, in recent years we have developed a novel technique to measure the attenuation curve in an independent manner, without assuming any functional form of the attenuation law. Our tests show that this method is able to obtain unbiased measurements of the attenuation curve from MaNGA-like IFS data.[17] This allows us to obtain a dust-free intrinsic model spectrum before performing stellar population synthesis modelling, thus largely breaking the degeneracies between dust attenuation and stellar populations. We have applied this method to the MaNGA data, and carried out a series of studies of galaxies at kpc scales on stellar initial mass function,[18–20] star formation histories,[21,22] and stellar and gaseous dust attenuations.[17,23]

In this paper we present our data produced by applying our spectral fitting technique to the final MaNGA data release (SDSS-DR17), including stellar and gas kinematics, emission line parameters, dust attenuation and stellar population properties for 10010 galaxies. We make the data publicly available to the community. We describe the MaNGA survey and our method in Section 2, describe the content and format of our data products in Section 3, and summarize the paper in Section 4. Throughout this paper we assume a Λ cold dark matter cosmology model with $\Omega_{\rm m} = 0.3$, $\Omega_\Lambda = 0.7$, and $H_0 = 70\ {\rm km\cdot s^{-1}\cdot Mpc^{-1}}$, and the stellar initial mass function (IMF) of Chabrier (2003).[24]

2. Data

2.1. Overview of MaNGA

The MaNGA survey[6] is one of the three core programs of the fourth-generation Sloan Digital Sky Survey project (SDSS-IV).[25] During its six-year observation from July 2014 through August 2020, MaNGA successfully obtained IFS for 10010 nearby galaxies using a set of 17 integral field units (IFUs), with five different sizes ranging from $12''$ to $32''$ in diameter. Each IFU is a hexagonal-formatted fiber bundle made from $2''$-core-diameter fibers with $0.5''$ gaps between adjacent fiber cores, producing IFS datacubes with an effective spatial resolution of $\sim 2.5''$.[26,27] The IFU fibers are fed to the BOSS spectrographs on the Sloan 2.5-meter telescope[28,29] to produce MaNGA spectra that cover a wavelength range from 3622 Å to 10354 Å with a spectral resolution ~ 2000. With a typical exposure time of three hours, the MaNGA spectra reach a target r-band signal-to-noise (SNR) of 4–8 (Å^{-1} per $2''$ fiber) at 1–2 effective radius ($R_{\rm e}$) of each galaxy.

Targets of the MaNGA survey are selected from the NASA Sloan Atlas (NSA), a catalog of ~ 640000 low-redshift galaxies constructed by Blanton *et al.* (2011)[30] based on data from SDSS, GALEX and 2MASS. As detailed in Wake *et al.* (2017),[31] the MaNGA sample selection is designed so as to simultaneously optimize the IFU size distribution, the IFU allocation strategy and the number density of targets. The primary and secondary samples, which are the main samples of the survey, are selected to effectively have a flat distribution of the K-corrected i-band absolute magnitude (M_i), and to be covered by MaNGA IFUs out to $1.5R_{\rm e}$ and $2.5R_{\rm e}$, respectively. In addition, the color-enhanced sample further selects galaxies that are not well sampled by the main samples in the NUV-r versus M_i diagram. Overall, the MaNGA targets cover a wide range of stellar mass, $10^9 M_\odot \lesssim M_* \lesssim 6\times 10^{11} M_\odot$, and a redshift range, $0.01 < z < 0.15$, with a median redshift of $z \sim 0.03$. Figure 1 displays the distribution of the final sample of MaNGA (the MaNGA Product Launch 11, or MPL11 in short) in the NUV-r versus stellar mass plane. For comparison, we have also selected from the NSA a volume-limited sample consisting of $\sim 3.5\times 10^4$ galaxies with stellar mass $M_* > 10^9 M_\odot$ and redshift in the range $0.01 < z < 0.03$. The distribution of this sample is plotted as the gray background in Fig. 1. As can be seen, the MaNGA sample is well representative of the general population of galaxies in the local universe.

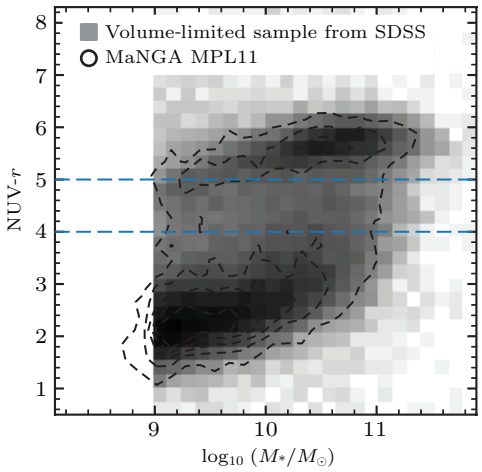


Fig. 1. Diagram of NUV-r color versus $\log_{10}(M_*/M_\odot)$. The black dashed contours show the distribution of the MaNGA MPL11 sample. The gray-scale distribution in the background is for a volume-limited sample of galaxies selected from the SDSS with $M_* > 10^9 M_\odot$ and $0.01 < z < 0.03$. The two horizontal dashed lines represent NUV-$r = 4$ and NUV-$r = 5$, which are often used to divided galaxies into blue, green and red in the color space.

MaNGA raw data are reduced using the Data Reduction Pipeline[9] to produce a datacube for each galaxy with a spaxel size of $0.5''\times 0.5''$ and absolute flux calibration better than 5% for most of the wavelength range.[32,33] The final data release from MaNGA includes DRP products of 11273 datacubes for 10010 unique galaxies in the MPL11, as part of the SDSS Data Release 17 (SDSS DR17).[10] Of the 11273 datacubes, there are 10145 high-quality galaxy observations discounting the Coma, IC342, M31, and globular cluster targets.

2.2. Stellar population models

There are several widely-used stellar population synthesis models.[34–36] In this paper, we use the simple stellar population (SSP) models from Bruzual & Charlot (2003, hereafter BC03).[34] Using the Bertelli *et al.* (1994)[37] evolutionary tracks and Chabrier (2003)[24] IMF, BC03 includes a total of 1326 SSPs at a spectral resolution of 3 Å, with 221 ages ranging from $t = 0$ yr to $t = 2\times10^{10}$ yr and six metallicities ranging from $Z = 0.0001$ to $Z = 0.05$ (note that the solar metallicity $Z_{\odot} = 0.02$).

In order to speed up some part of the fitting processes, we follow the method of Li *et al.* (2005)[38] and construct a small set of model templates by applying the technique of principal component analysis (PCA)[39] to the BC03 SSPs. PCA can effectively reduce the size of the template library, as the principal features of the library can be described by the first few eigenspectra. In our analysis, we apply the PCA to the 1326 BC03 SSPs, and we adopt the first 9 eigenspectra that resulted from the PCA as the model templates to fit the spectra when measuring stellar and gas kinematics, flux of emission lines and dust attenuation. The cumulative contribution to variance by the first 9 eigenspectra is 99.96%, indicating that they contain nearly all the information of the original 1326 SSPs.

2.3. Measuring stellar kinematics

Stars in different regions of galaxies usually have different motions that can be characterized by stellar velocity v_* and stellar velocity dispersion σ_*. Firstly, we use a Gaussian distribution $G(v_*, \sigma_*)$ centred at v_* and with dispersion σ_* to model the stellar motions along line of sight. For a given spectrum $F(\lambda)$, we fit it with the 9 PCA eigenspectra

$$F(\lambda) = \left(\sum_{j=1}^{j=9} x_j f^j_{\rm PCA}(\lambda) A(\lambda)\right) \otimes G(v_*, \sigma_*), \qquad (1)$$

where $f^j_{\rm PCA}(\lambda)$ is the j-th eigenspectrum, x_j is the coefficient of the eigenspectrum, $A(\lambda)$ is the attenuation curve, and $\otimes$ denotes the convolution operator. In this paper, we use the Calzetti *et al.* (2000)[40] attenuation curve by default and we have carefully masked out all the detected emission lines in the observed spectra during fitting, following the scheme described in Li *et al.* (2005).[38] We do not consider the line spread function (LSF) of the instrument of MaNGA as the spectral resolution of the eigenspectra corresponding to a median resolving power of $R = \lambda/\Delta\lambda \approx 2000$ is comparable to the spectral resolution of MaNGA ~ 2000. Figure 2 shows an example to display the spectral fitting of our code. Spectral pixels at wavelength larger than 8000 Å are masked due to low signal-to-noise in this range, especially in the outer regions of galaxies.

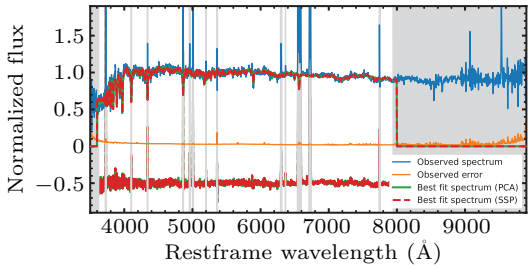


Fig. 2. An example of the full spectral fitting. This spectrum is taken from the MaNGA datacube for galaxy '7443-12703' with the spaxel coordinate (25, 35). The blue line shows the observed spectrum which is normalized to have a flux of unity at 5500 Å. The orange line is the observed error spectrum. The green line shows the best-fit model spectrum using the 9 PCA eigenspectra, and the red line shows the best-fit model spectrum using the 150 SSPs (Note the two lines almost completely overlap). The grey shaded areas indicate the wavelength ranges that are masked out during the fitting. The red and green lines in the bottom are the residual spectra, that is, the difference between the observed and the best-fit spectra. For clarity, the residual spectra are shifted vertically by −0.5.

2.4. Measuring emission lines

We then measure the flux, equivalent width, velocity and velocity dispersion of emission lines. We include 20 widely-considered lines in the optical, such as Hα, Hβ, [O III]$\lambda\lambda$4959, 5007 Å, [N II]$\lambda\lambda$6548, 6583 Å, [S II]$\lambda\lambda$6717, 6731 Å, etc. We subtract the best-fit stellar spectrum obtained in Subsection 2.3 from the observed spectrum, and fit the emission lines each with a Gaussian profile. The line ratios of [N II]λ6583/N II]λ6548 and [O III]λ5007/[O III]λ4959 are fixed to 3 during the fitting. The parameters of each line are then calculated from the Gaussian profiles, together with the best-fit stellar spectrum when needed.

2.5. Measuring stellar attenuation

For each observed spectrum we estimate the relative attenuation curve, $(A_\lambda - A_V)$, and the stellar color excess, $E(B-V) \equiv A_B - A_V$, by applying the method developed in Li *et al.* (2020),[17] where A_V and A_B are dust attenuation at V-band ($\lambda_V = 5500$ Å) and B-band ($\lambda_B = 4400$ Å), respectively. In this method, the small-scale features (S) in the observed spectrum is firstly separated from the large-scale spectral shape (L) using a moving average filter. The same separation is also performed for the 9 PCA eigenspectra, and the intrinsic dust-free model spectrum of the stellar component is then derived by fitting the observed ratio of the small- to large-scale spectral components $(S/L)_{\rm obs}$ with the same ratio of the model spectra $(S/L)_{\rm model}$. The effect of the stellar velocity and stellar velocity dispersion is taken into account by convolving $G(v_*, \sigma_*)$ obtained above (see Eq. (1)) before the spectral decomposition. As shown in Li *et al.* (2020)[17] (see subsection 2.1 and Eqs. (3)–(8) in that paper), the small- and large-scale components are attenuated by dust in the same way so that their ratio S/L is dust-free, as long as the dust attenuation curves are similar for different stellar populations in a galactic region. Finally, $A_\lambda - A_V$ is derived by comparing the observed spectrum with the best-fit model spectrum. The value of $E(B-V)$ is

then directly calculated from $(A_\lambda - A_V)$.

As shown in Li *et al.* (2020),[17] one important advantage of this method is that the relative dust attenuation curve can be directly obtained without the need to assume a functional form for the curve. Furthermore, extensive tests on mock spectra have shown that the method is able to recover the input dust attenuation curve accurately from an observed spectrum with SNR > 5, as long as the underlying stellar populations have similar dust attenuation or the optical depths are smaller than unity. Figures 3(a) and 3(b) display the small- to large-scale spectral fitting and the obtained relative attenuation curve for the observed spectrum shown in Fig. 2. Figure 3(c) shows the results of the tests with mock spectra that are constructed in Li *et al.* (2020).[17] It can be seen that the distribution of $\Delta E(B-V)$, defined to be the difference between the output and input $E(B-V)$, is roughly a Gaussian centered at $\Delta E(B-V) \sim 0$ with a scatter decreasing with increasing SNR. Our method provides unbiased measurements of $E(B-V)$ with no systematics for $E(B-V) > 0.05$ and SNR> 5.

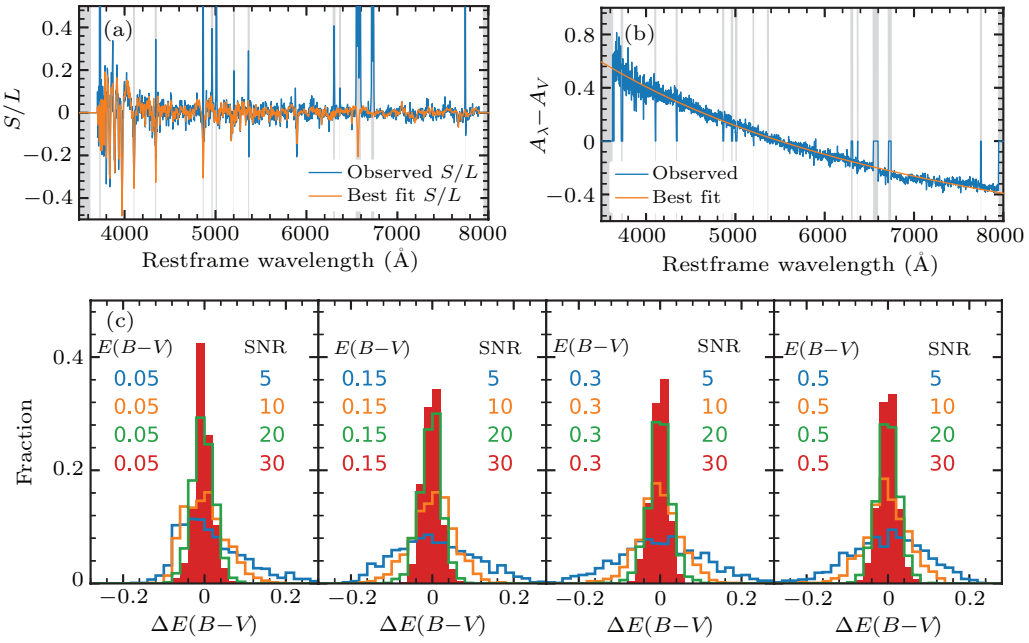


Fig. 3. (a) The small- to large-scale spectral fitting (S/L) of spectrum in Fig. 2. (b) The obtained relative attenuation curve of spectrum in Fig. 2. (c) Tests with mock spectra that have different $E(B-V)$ and SNR as indicated. The histograms show the distribution of $\Delta E(B-V)$, which means the difference between the fitting result of $E(B-V)$ and the input value. The data of the results are from Li *et al.* (2020).[17]

2.6. Measuring stellar populations

Using the measurements of v_*, σ_* and $E(B-V)$ obtained above, we correct the effect of stellar motions and dust attenuation for each spectrum. We then measure stellar population parameters by performing full spectral fitting to the dust-free spectrum with zero velocity broadening. We select a subset of 150 SSPs from BC03 that cover 25 ages at each of the six metallicities, ranging from $t = 0.001$ Gyr to $t = 13$ Gyr with approximately equal intervals in $\log_{10} t$. For a given spectrum, we fit the spectrum $F(\lambda)$ with a linear combination of the SSPs:

$$F(\lambda) = \sum_{j=1}^{j=150} x_j f^j_{\rm SSP}(\lambda), \qquad (2)$$

where $f^j_{\rm SSP}(\lambda)$ is the spectrum of the j-th SSP, and x_j is the coefficient of the j-th SSP to be determined by the fitting. We then obtain the parameters to quantify the stellar populations for each spectrum, based on the coefficients x_j of the best-fit stellar spectrum or the best-fit spectrum itself such as stellar mass, stellar age and stellar metallicity.

3. Data products

The datacubes produced by the MaNGA DRP are three-dimensional arrays, in which the first and second dimensions form the two-dimensional map of spatial pixels (spaxels) with a spaxel size of $0.5'' \times 0.5''$ (NX$\times$NY spaxels) and the third dimension represents wavelength pixels. The fitting/measuring process described in the previous section is performed for each spaxel separately, and the derived parameters are stored also in the form of three-dimensional arrays, for each of which we keep the data in the first two dimensions (the spaxel coordinates) but use the third dimension for one of the derived parameters. For a given galaxy, all the three-dimensional arrays are stored in a single fits-format file, contained separately in 35 data extensions as listed in Table 1. Data files are named as 'manga-plate-ifu-MAPS2.fits.gz', where 'plate-ifu' is the MaNGA ID for a given galaxy. For example, the file name for the MaNGA galaxy '7443-12703' is 'manga-7443-12703-MAPS2.fits.gz'. As an example, Fig. 4 displays the maps of some parameters for MaNGA galaxy '7443-12703'.

Below are more details for some of the data extensions listed in Table 1.

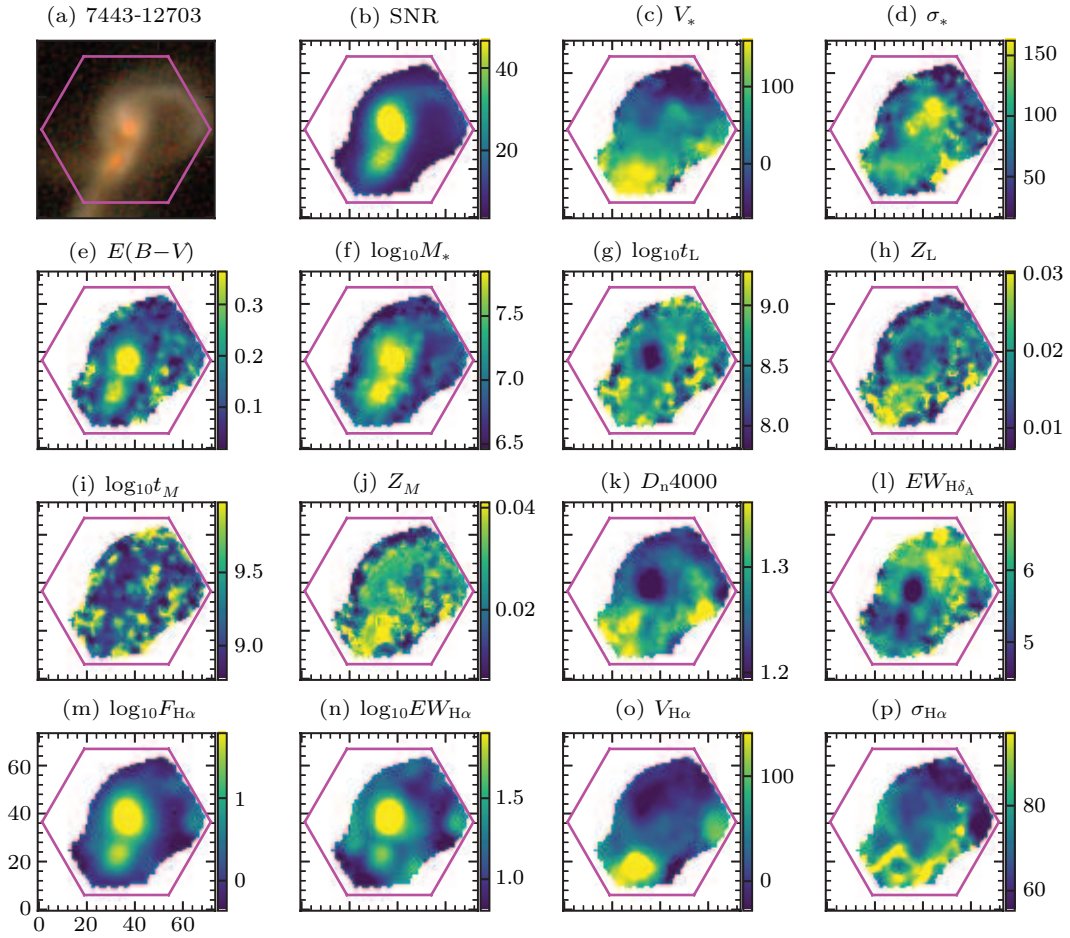


Fig. 4. An example to show the maps of our main measurements. (a) The *gri* color composite image of MaNGA galaxy '7443-12703'. (b) Signal-to-noise ratio of the spectra. (c) Stellar velocity. (d) Stellar velocity dispersion. (e) Color excess $E(B-V)$. (f) Stellar mass. (g) Light-weighted stellar age. (h) Light-weighted stellar metallicity. (i) Mass-weighted stellar age. (j) Mass-weighted stellar metallicity. (k) 4000 Å break. (l) Equivalent width of Hδ absorption. (m) Hα flux. (n) Equivalent width of Hα. (o) Velocity of Hα. (p) Velocity dispersion of Hα. x and y axes indicate the number of spaxels whose size is $0.5'' \times 0.5''$. For clarity, we only show them in the lower left panel.

Table 1. Extensions of 'manga-plate-ifu-MAPS2.fits.gz'.

	Name	Units	Description		Name	Units	Description
0			header of DRP flux	18	z_L2	$Z_\odot = 0.02$	light-weighted metallicity
1	snr		signal-to-noise ratio	19	age_M2	$\log_{10}$ [yr]	mass-weighted age
2	nor		normalization coefficient	20	z_M2	$Z_\odot = 0.02$	mass-weighted metallicity
3	ve	km/s	stellar velocity	21	wei		weights of 9 eigenspectra
4	ve_err	km/s	error of ve	22	p12		coefficients of $A_\lambda - A_V$
5	vd	km/s	stellar velocity dispersion	23	emlines_center	Å	emission lines' center
6	vd_err	km/s	error of vd	24	emlines_center_err	Å	error of emlines_center
7	weights		weights of 150 SSPs	25	emlines_sigma	Å	emission lines' dispersion
8	ebv	mag	color excess $E(B-V)$	26	emlines_sigma_err	Å	error of emlines_sigma
9	ebv_err	mag	error of ebv	27	emlines_flux	erg/s/cm^2	emission lines' flux $\times 10^{17}$
10	dof		degree of freedom in fitting	28	emlines_flux_err	erg/s/cm^2	error of emlines_flux $\times 10^{17}$
11	chi2		chi-square of the fitting	29	emlines_ew	Å	equivalent width
12	M	$M_\odot$	stellar mass	30	emlines_ew_err	Å	error of emlines_ew
13	age_L	$\log_{10}$ [yr]	light-weighted age	31	d4000_n		4000 Å break D_n4000
14	z_L	$Z_\odot = 0.02$	light-weighted metallicity	32	d4000_n_err		error of d4000_n
15	age_M	$\log_{10}$ [yr]	mass-weighted age	33	lick_hd_a	Å	equivalent width of Hδ_A
16	z_M	$Z_\odot = 0.02$	mass-weighted metallicity	34	lick_hd_a_err	Å	error of lick_hd_a
17	age_L2	$\log_{10}$ [yr]	light-weighted age				

• Extension 0 — No data is stored in this extension. The header is the same as that of the 'FLUX' extension of DRP datacubes.

• Extension 1: 'snr' (NX×NY) — Signal-to-noise ratio of the spectrum defined by the total flux to total error ratio of unmasked wavelength pixels in the fitting. Spectra with SNR < 3 are skipped during our spectral fitting, and data for such spectra should be ignored.

• Extension 2: 'nor' (NX×NY) — Normalization coefficient. We normalize the spectra at 5500 Å before perform-

ing the spectral fitting so as to avoid computer value overflow. This normalization is taken into account when calculating stellar mass and measuring emission lines.

• Extension 3: 've' (NX×NY) — Stellar velocity in units of km/s. We have corrected the spectra to the restframe using redshift from the NSA, which can be found as 'z' in the header of extension 0.

• Extension 7: 'weights' (NX×NY×150) — Weights of the 150 SSPs with which the best-fit stellar model spectrum is formed, as detailed in Subsection 2.6.

• Extension 8: 'ebv' (NX×NY) — $E(B-V)$ measured by our method as described in Subsection 2.5.

• Extension 12: 'M' (NX×NY) — Stellar mass given by $M=\sum_{j=1}^{150}x_jM_j$ in units of $M_\odot$, where M_j is the stellar mass of the j-th SSP.

• Extension 13: 'age_L' (NX×NY) — Logarithm of the light-weighted stellar age, given by $\log_{10}t_{\rm L}=\sum_{j=1}^{150}x_j\log_{10}t_j$, where t_j is the age of the j-th SSP in units of yr.

• Extension 14: 'z_L' (NX×NY) — Light-weighted stellar metallicity, given by $Z_{\rm L}=\sum_{j=1}^{150}x_jZ_j$, where Z_j is the metallicity of the j-th SSP. Note that stellar metallicity $Z_\odot=0.02$.

• Extension 15: 'age_M' (NX×NY) — Logarithm of the mass-weighted stellar age, given by $\log_{10}t_M=(\sum_{j=1}^{150}x_jM_j\log_{10}t_j)/(\sum_{j=1}^{150}x_jM_j)$.

• Extension 16: 'z_M' (NX×NY) — Mass-weighted stellar metallicity, given by $Z_M=(\sum_{j=1}^{150}x_jM_jZ_j)/(\sum_{j=1}^{150}x_jM_j)$.

• Extension 17: 'age_L2' (NX×NY) — Logarithm of the light-weighted stellar age, given by $\log_{10}t_{\rm L2}=\log_{10}(\sum_{j=1}^{150}x_jt_j)$.

• Extension 18: 'z_L2' (NX×NY) — Light-weighted stellar metallicity, given by $\log_{10}Z_{\rm L2}=\sum_{j=1}^{150}x_j\log_{10}Z_j$.

• Extension 19: 'age_M2' (NX×NY) — Logarithm of the mass-weighted stellar age, given by $\log_{10}t_{M2}=\log_{10}((\sum_{j=1}^{150}x_jM_jt_j)/(\sum_{j=1}^{150}x_jM_j))$.

• Extension 20: 'z_M2' (NX×NY) — Mass-weighted stellar metallicity, given by $\log_{10}Z_{M2}=(\sum_{j=1}^{150}x_jM_j\log_{10}Z_j)/(\sum_{j=1}^{150}x_jM_j)$.

• Extension 21: 'wei' (NX×NY×9) — Weights of the 9 PCA eigenspectra that used to fit S/L as described in Subsection 2.5.

• Extension 22: 'p12' (NX×NY×2) — Coefficients of best fit $A_\lambda-A_V$ curve, given by $A_\lambda-A_V=p_1\times10000/\lambda+p_2\times(10000/\lambda)^2-p_1\times10000/\lambda_V-p_2\times(10000/\lambda_V)^2$, where $\lambda_V=5500$ Å.

• The extensions 23–30 contain 22 channels of emission lines whose names can be found in the header of those extensions. Note that 'Ha6563_b' and 'Hb4861_b' are broad components of Hα and Hβ if detected.

• Extension 23: 'emlines_center' (NX×NY×22) — We have corrected stellar velocity when using the Gaussian profiles to fit each emission lines. Thus velocity of emission lines should be $v_{\rm line}=c\times(\lambda_0-\lambda_{\rm line})/\lambda_{\rm line}+v_*$, where λ_0 is the best fit center of the emission line, $\lambda_{\rm line}$ is the vacuum wavelength of the emission line, v_* is stellar velocity and c is the speed of light.

• Extension 25: 'emlines_sigma' (NX×NY×22) — The velocity dispersion of emission lines should be $\sigma_{\rm line}=c\times\sigma/\lambda_{\rm line}$, where σ is the best fit dispersion of the Gaussian profile.

• Extension 27: 'emlines_flux' (NX×NY×22) — Note that the unit is $10^{-17}{\rm erg/s/cm^2}$.

• Extension 29: 'emlines_ew' (NX×NY×22) — Equivalent width of emission lines.

• Extension 31: 'd4000_n' (NX×NY) — The narrow-band version of the 4000 Å break, defined by Balogh *et al.* (1999).[41]

• Extension 33: 'lick_hd_a' (NX×NY) — Equivalent width of Hδ absorption.

As mentioned above, the header of extension 0 is copied from the 'FLUX' extension of DRP datacubes which contains information about the DRP version, coordinate system, observation conditions, etc. For other extensions, the headers also contain the information of the coordinate system, so that one can calculate the RA and DEC for a given spaxel. Here we list some important keywords of the header. For more details about these keywords and on how to use them in practice, one can visit the SDSS website.

• 'OBJRA' — right ascension (RA) of the galaxy center in units of degrees.

• 'OBJDEC' — declination (DEC) of the galaxy center in units of degrees.

• 'IFURA' — RA of the IFU pointing center in units of degrees.

• 'IFUDEC' — DEC of the IFU pointing center in units of degrees.

• 'CRVAL1' — RA of the reference point. It is the same with 'IFURA' in units of degrees.

• 'CRVAL2' — DEC of the reference point. It is the same with 'IFUDEC' in units of degrees.

• 'CRPIX1' — pixel coordinate of reference point in the first dimension. It corresponds to 'CRVAL1' and is indexed from 1.

• 'CRPIX2' — pixel coordinate of reference point in the second dimension. It corresponds to 'CRVAL2' and is indexed from 1.

• 'CD1_1' or 'PC1_1' — the gradient of pixel coordinate in the first dimension. It is $-0.5''$ for MaNGA datacubes.

• 'CD2_2' or 'PC2_2' — the gradient of pixel coordinate in the second dimension. It is $0.5''$ for MaNGA datacubes.

• 'Z' — redshift of the galaxy from the NSA. We additionally add this keyword.

4. Summary

In the past few years, we have made lots of efforts to develop a novel technique of full spectral fitting. One important advantage of this method is that the estimated dust

attenuation curve is independent of the shape of theoretical dust attenuation curves, thus allowing us to break the degeneracy between dust attenuation and stellar population properties when performing full spectral fitting. As detailed in Li *et al.* (2020),[17] we have carried out a series of tests on a set of mock spectra covering wide ranges of stellar age and metallicity, showing that our method is able to recover the input dust attenuation curves accurately. We have applied this method to the MaNGA data and published a series of studies on the resolved properties of nearby galaxies including stellar initial mass function, star formation histories, and stellar and gaseous dust attenuations.[17–23]

MaNGA has finished its observation in August 2020 and all the datacubes processed by the MaNGA DRP have been publicly released as part of SDSS DR17.[10] In this paper, we apply our spectral fitting technique to the final data release of MaNGA, which include 10010 unique galaxies. We have obtained measurements of stellar population properties and emission line parameters, as well as the kinematics and dust attenuation of both stellar and ionized gas components. We describe the content and format of our data products, and we would like to share all our data products with the community.

Data availability statement

The data that support the findings of this study are openly available in Science Data Bank at https://doi.org/10.57760/sciencedb.j00113.00088.

Acknowledgements

This work is supported by the National Key R&D Program of China (Grant No. 2018YFA0404502), and the National Natural Science Foundation of China (Grant Nos. 11821303, 11733002, 11973030, 11673015, 11733004, 11761131004, and 11761141012).

Funding for the Sloan Digital Sky Survey IV has been provided by the Alfred P. Sloan Foundation, the U.S. Department of Energy Office of Science, and the Participating Institutions. SDSS-IV acknowledges support and resources from the Center for High-Performance Computing at the University of Utah. The SDSS web site is www.sdss.org.

SDSS-IV is managed by the Astrophysical Research Consortium for the Participating Institutions of the SDSS Collaboration including the Brazilian Participation Group, the Carnegie Institution for Science, Carnegie Mellon University, the Chilean Participation Group, the French Participation Group, Harvard-Smithsonian Center for Astrophysics, Instituto de Astrofísica de Canarias, the Johns Hopkins University, Kavli Institute for the Physics and Mathematics of the Universe (IPMU) / University of Tokyo, Lawrence Berkeley National Laboratory, Leibniz Institut für Astrophysik Potsdam (AIP), Max-Planck-Institut für Astronomie (MPIA Heidelberg), Max-Planck-Institut für Astrophysik (MPA Garching), Max-Planck-Institut für Extraterrestrische Physik (MPE), National Astronomical Observatories of China, New Mexico State University, New York University, University of Notre Dame, Observatário Nacional / MCTI, the Ohio State University, Pennsylvania State University, Shanghai Astronomical Observatory, United Kingdom Participation Group, Universidad Nacional Autónoma de México, University of Arizona, University of Colorado Boulder, University of Oxford, University of Portsmouth, University of Utah, University of Virginia, University of Washington, University of Wisconsin, Vanderbilt University, and Yale University.

References

[1] Bacon R, Copin Y, Monnet G, *et al*. 2001 *MNRAS* **326** 23
[2] Bershady Matthew A, Verheijen Marc A W, Swaters Rob A, *et al*. 2010 *ApJ* **716** 198
[3] Cappellari M, Emsellem E, Krajnović D, *et al*. 2011 *MNRAS* **416** 1680
[4] Croom Scott M, Lawrence Jon S, Bland-Hawthorn J, *et al*. 2012 *MNRAS* **421** 872
[5] Sánchez S F, Kennicutt R C, Gil de Paz A, *et al*. 2012 *A&A* **538** 8
[6] Bundy K, Bershady M A, Law D R, *et al*. 2015 *ApJ* **798** 7
[7] Poggianti Bianca M, Moretti Alessia, Gullieuszik Marco, *et al*. 2017 *ApJ* **844** 48
[8] Emsellem E, Schinnerer E, Santoro F, *et al*. 2022 *A&A* **659** 191
[9] Law D R, Cherinka B, Yan R, *et al*. 2016 *AJ* **152** 83
[10] Abdurro'uf, Accetta K, Aerts C, *et al*. 2022 *ApJS* **259** 35
[11] Westfall Kyle B, Cappellari M, Bershady Matthew A, *et al*. 2019 *AJ* **158** 231
[12] Cappellari M and Emsellem E 2004 *PASP* **116** 138
[13] Cid Fernandes R, Mateus A, Sodré L, *et al*. 2005 *MNRAS* **358** 363
[14] Sánchez S F, Pérez E, Sánchez-Blázquez P, *et al*. 2016 *RMxAA* **52** 21
[15] Wilkinson D M, Maraston C, Thomas D, *et al*. 2015 *MNRAS* **449** 328
[16] Wilkinson D M, Maraston C, Goddard D, *et al*. 2017 *MNRAS* **472** 4297
[17] Li N, Li C, Mo H J, *et al*. 2020 *ApJ* **896** 38
[18] Zhou S, Mo H J, Li C, *et al*. 2019 *MNRAS* **485** 5256
[19] Liang F H, Li C, Li N, *et al*. 2020 *ApJ* **896** 121
[20] Liang F H, Li C, Li N, *et al*. 2021 *ApJ* **923** 120
[21] Zhou S, Mo H J, Li C, *et al*. 2020 *MNRAS* **497** 4753
[22] Zhou S, Mo H J, Li C, *et al*. 2021 *ApJ* **916** 38
[23] Li N, Li C, Mo H J, *et al*. 2021 *ApJ* **917** 72
[24] Chabrier G 2003 *PASP* **115** 763
[25] Blanton M R, Bershady M A, Abolfathi B, *et al*. 2017 *AJ* **154** 28
[26] Drory N, MacDonald N, Bershady M A, *et al*. 2015 *AJ* **149** 77
[27] Law David R, Yan R, Bershady Matthew A, *et al*. 2015 *AJ* **150** 19
[28] Gunn James E, Siegmund Walter A, Mannery Edward J, *et al*. 2006 *AJ* **131** 2332
[29] Smee Stephen A, Gunn James E, Uomoto A, *et al*. 2013 *AJ* **146** 32
[30] Blanton Michael R, Kazin E, Muna D, *et al*. 2011 *AJ* **142** 31
[31] Wake D A, Bundy K, Diamond-Stanic A M, *et al*. 2017 *AJ* **154** 86
[32] Yan R, Tremonti C, Bershady M A, *et al*. 2016 *AJ* **151** 8
[33] Yan R, Bundy K, Law D R, *et al*. 2016 *AJ* **152** 197
[34] Bruzual G and Charlot S 2003 *MNRAS* **344** 1000
[35] Maraston C 2005 *MNRAS* **362** 799
[36] Vazdekis A, Sánchez-Blázquez P, Falcón-Barroso J, *et al*. 2010 *MNRAS* **404** 1639
[37] Bertelli G, Bressan A, Chiosi C, *et al*. 1994 *A&A* **106** 275
[38] Li C, Wang T G, Zhou H Y, *et al*. 2005 *AJ* **129** 669
[39] Deeming T J 1964 *MNRAS* **127** 493
[40] Calzetti D, Armus L, Bohlin R C, *et al*. 2000 *ApJ* **533** 682
[41] Balogh Michael L, Morris Simon L, Yee H K C, *et al*. 1999 *ApJ* **527** 54